communications physics

A Nature Portfolio journal

Article

https://doi.org/10.1038/s42005-025-02225-8

Impact of charge-density-wave pattern on the superconducting gap in Vanadium-based kagome superconductors

Takuya Nagashima [1,7], Kota Ishihara [1,7] ✉, Youichi Yamakawa [2], Fan Chen[1], Kumpei Imamura[1], Masaki Roppongi [1], Romain Grasset [3], Marcin Konczykowski [3], Brenden R. Ortiz [4], Andrea Capa Salinas[5], Stephen D. Wilson [5], Rina Tazai [6], Hiroshi Kontani [2], Kenichiro Hashimoto [1] & Takasada Shibauchi [1] ✉

Kagome metals AV_3Sb_5 (A = K, Rb, Cs) provide a compelling platform to explore the interplay between superconductivity (SC) and charge-density-wave (CDW) orders. While distinct CDW orders have been identified in K/RbV_3Sb_5 versus CsV_3Sb_5, their influence on the SC order parameter remains unresolved. Here, we investigate low-energy quasiparticle excitations in AV_3Sb_5, uncovering a striking difference in SC gap anisotropy: K/RbV_3Sb_5 exhibit fully gapped, nearly isotropic s-wave states, in contrast to the strongly anisotropic SC gap in CsV_3Sb_5. Impurity scattering introduced via electron irradiation in K/RbV_3Sb_5 has a minimal impact on low-energy excitations, and it induces an increase in the SC transition temperature T_c, consistent with more isotropic s-wave SC competing with CDW order. Our theoretical analysis attributes the observed SC gap anisotropy differences to distinct CDW modulation patterns: the star-of-David structure unique to CsV_3Sb_5 preserves van Hove singularities near the Fermi level, promoting anisotropic s-wave SC with enhanced T_c via bond-order fluctuations. These findings establish a systematic framework for understanding the interplay between SC and CDW orders in AV_3Sb_5, driven by electron correlations.

Kagome lattices, two-dimensional networks of corner-sharing triangles, offer fertile playgrounds for various quantum phases due to their intrinsic geometrical frustrations and unique band structures, including flat bands, Dirac cones at K points, and van Hove singularities (vHSs) at M points. Especially when the Fermi level is located near vHSs, the divergent density of states (DOS), good nesting between M points, and characteristic orbital nature of vHSs give rise to a wide variety of emergent exotic orders such as spin-density-wave, CDW, loop-current orders, and unconventional SC[1–5]. Furthermore, recent efforts have been devoted to exploring novel emergent physics originating from an interplay between fascinating orders in kagome materials.

Recently discovered kagome metals AV_3Sb_5 (A = K, Rb, Cs), consisting of perfect kagome networks of V atoms (Fig. 1a), have attracted considerable attention due to their band structure with the Fermi energy situated near vHSs at M points[6]. In all alkali compounds, CDW and SC orders coexist with the CDW transition temperature T_{CDW} of 78, 104, and 94 K and the SC transition temperature T_c of 0.9, 0.8, and 2.5 K for A = K, Rb, and Cs, respectively[7–9]. A strong interplay between the SC and CDW orders is implied from the pressure-temperature (P-T) phase diagram, where T_c shows a peak structure around the CDW endpoint[10–13]. The CDW order is expected to be quite exotic, with time-reversal symmetry (TRS)[14–19] and rotational symmetry[18–24] breaking, as well as translational symmetry breaking. The coexistence of bond order (BO) and loop-current order, where the former corresponds to a real CDW order that preserves TRS and the latter corresponds to an imaginary CDW order that breaks TRS, has been theoretically proposed to understand the multiple symmetry breaking in kagome metals[5,25].

Although the overall band structure is similar in all alkali compounds, some differences in electronic states between K/RbV_3Sb_5 and CsV_3Sb_5 have been recently pointed out[6]. For example, although the BO within the

[1]Department of Advanced Materials Science, University of Tokyo, Kashiwa, Chiba, Japan. [2]Department of Physics, Nagoya University, Nagoya, Japan. [3]Laboratoire des Solides Irradiés, CEA/DRF/IRAMIS, Ecole Polytechnique, CNRS, Institut Polytechnique de Paris, Palaiseau, France. [4]Materials Science and Technology Division, Oak Ridge National Laboratory, Oak Ridge, TN, USA. [5]Materials Department, University of California Santa Barbara, Santa Barbara, CA, USA. [6]Yukawa Institute for Theoretical Physics, Kyoto University, Kyoto, Japan. [7]These authors contributed equally: Takuya Nagashima, Kota Ishihara.
✉e-mail: k.ishihara@edu.k.u-tokyo.ac.jp; shibauchi@k.u-tokyo.ac.jp

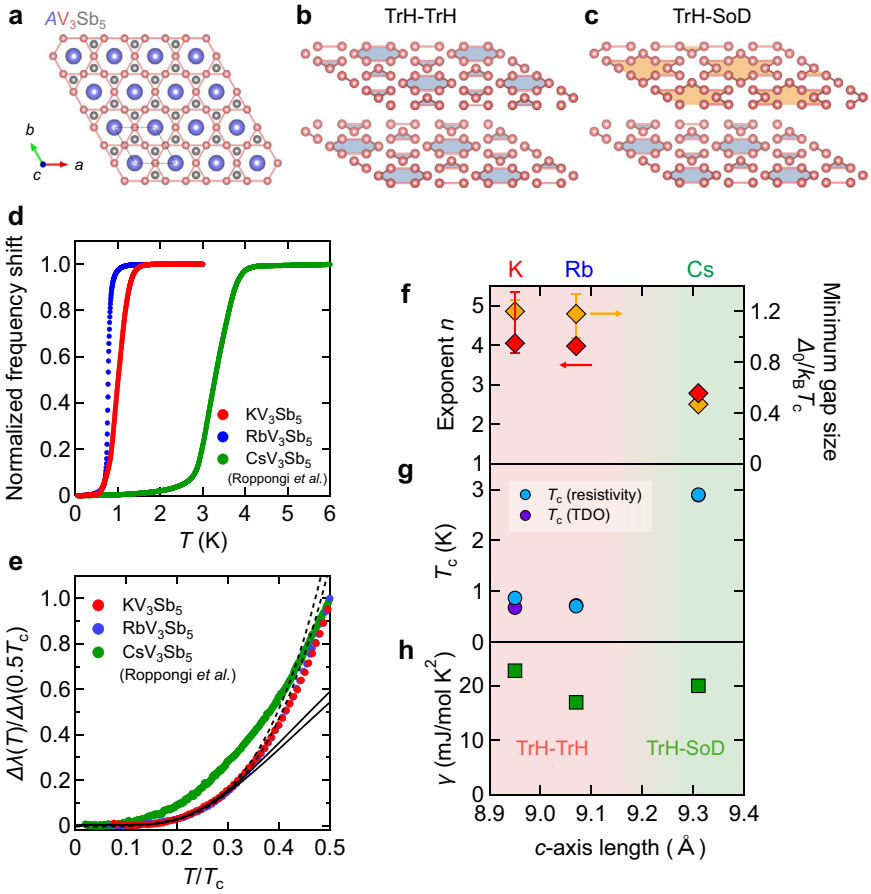

Fig. 1 | Crystal structure, charge-density-wave (CDW) modulations, and penetration depth measurements in AV_3Sb_5 (A = K, Rb, Cs). **a** Crystal structure of AV_3Sb_5. The three-dimensional bond-order structure in AV_3Sb_5: trihexagonal (TrH) order with π phase shift between neighboring planes (**b**), and a mixture of TrH and star of David (SoD) orders (**c**). **d** Temperature dependence of the normalized frequency shift of the tunnel diode oscillator(TDO) for the pristine samples of AV_3Sb_5. The data for CsV_3Sb_5 are taken from ref. 37. **e** Temperature dependence of the penetration depth below $0.5T_c$ normalized by the value at $0.5T_c$ for the pristine samples of AV_3Sb_5. The black dashed lines and black solid lines represent fitting curves with power-law and fully-gapped models, respectively. **f** Exponent n obtained from the fitting with power-law below $0.3T_c$ (red diamonds), minimum gap size Δ_0/k_BT_c obtained from the fully-gapped fitting (orange diamonds) as a function of c-axis length, where Δ_0 is the gap minima, k_B is the Boltzmann constant, and T_c is the superconducting transition temperature. The error bar is estimated by varying the fitting range $0.25 \le T_{max}/T_c \le 0.35$, where T_{max} is the maximum temperature of the fitting range (see Supplementary Note 2). **g** T_c determined from the resistivity measurements by linearly extrapolating the resistivity in the transition region to zero (light blue circles), and from the TDO measurements, where superfluid density becomes finite (purple circles). **h** Sommerfeld coefficient γ obtained from the specific heat measurements[8,9,41].

kagome planes is established as the 2 × 2 star of David (SoD) or trihexagonal (TrH) structure by scanning tunneling microscopy (STM) measurements[15,20,26], the out-of-plane modulation pattern of the BO varies between K/RbV_3Sb_5 and CsV_3Sb_5. Specifically, 2 × 2 × 2 staggered TrH order with π phase shift (Fig. 1b) is expected in K/RbV_3Sb_5[27–30], and 2 × 2 × 2 and 2 × 2 × 4 more complex patterns with coexisting SoD and TrH orders (Fig. 1c) are discussed in CsV_3Sb_5[27,28,31–33]. Indeed, differences in the momentum-dependent CDW gap and structural deformations associated with the CDW transition have been detected by angle-resolved photoemission spectroscopy (ARPES) and x-ray diffraction measurements between K/RbV_3Sb_5 and CsV_3Sb_5[27,28]. As the origin of the distinct CDW patterns, the involvement of vHSs having different orbital characters below the Fermi energy has been theoretically discussed[6]. It is noteworthy that, in the P-T and hole-doping $AV_3Sb_{5-x}Sn_x$ phase diagrams, the SC phase shows a single peak at the CDW endpoint in A = K and Rb[10,11,34], while in A = Cs it shows double peaks: one within the CDW phase and the other at the CDW endpoint[12,13,35]. These distinct peak structures are likely associated with the different CDW patterns between K/RbV_3Sb_5 and CsV_3Sb_5, and subsequent changes in the CDW state under pressure or hole-doping in CsV_3Sb_5[27,36].

As for the SC symmetry, theories based on AV_3Sb_5 have proposed the spin-triplet p- and f-wave, spin-singlet chiral d-wave, and nodal or nodeless s-wave states[1–4]. From the experimental point of view, some of the authors have reported systematic penetration depth measurements by changing the impurity concentrations in CsV_3Sb_5, indicating an anisotropic nodeless s-wave pairing without sign change in the gap function[37], in line with nuclear quadrupole resonance[38], muon spin relaxation (μSR)[39], STM[40], and similar penetration depth measurements[41,42]. Especially a recent ARPES study on CsV_3Sb_5 reported the coexistence of anisotropic and isotropic SC gaps in the momentum space[43], which confirms the validity of two-band model used in ref. 37. On the other hand, the gap structure in K/RbV_3Sb_5 has been rarely investigated except for a μSR study suggesting a nodal gap structure from a linear-in-T behavior of the superfluid density at low temperatures[44]. Thus, a systematic understanding of the SC gap structure in the AV_3Sb_5 family and the relationship between the SC and CDW orders remain elusive.

The interplay between the SC and CDW orders in AV_3Sb_5 has been studied through the phase diagrams under pressure or chemical substitutions[10–13,34,35]. However, these approaches alter the lattice constants, resulting in a change in the band structures, which may mask a pure interrelation between the SC and CDW orders. In this study, we instead focus on impurity effects on the SC and CDW states, which have been applied to study the relationship between SC and CDW orders in cuprates and transition metal dichalcogenides (TMDs) without affecting the crystal and electronic structure[45,46]. Furthermore, impurity effects are quite useful to investigate the SC symmetry because the conventional SC is robust against nonmagnetic impurities, while unconventional SC states with strong gap anisotropy can be suppressed by disorder[37]. Moreover, nonmagnetic impurity scatterings induce additional low-energy Andreev bound states when the gap function has a sign change, which can be detected by low-energy quasiparticle excitation measurements[47,48]. Therefore, the combination of measurements of quasiparticle excitations and their impurity effects is a phase-sensitive bulk probe of the gap symmetry, which can distinguish, for example, fully-gapped s-wave and chiral d-wave pairings. In this study, we performed magnetic penetration depth measurements by the tunnel diode oscillator (TDO) technique combined with a systematic control of impurity concentrations using high-energy electron irradiation in K/RbV_3Sb_5 to provide a comprehensive understanding of the SC symmetry and the interplay between the SC and CDW orders in the AV_3Sb_5 family.

Results

Magnetic penetration depth

First, we discuss the SC gap structure of AV_3Sb_5 from the temperature dependence of the penetration depth in pristine samples. Figure 1d

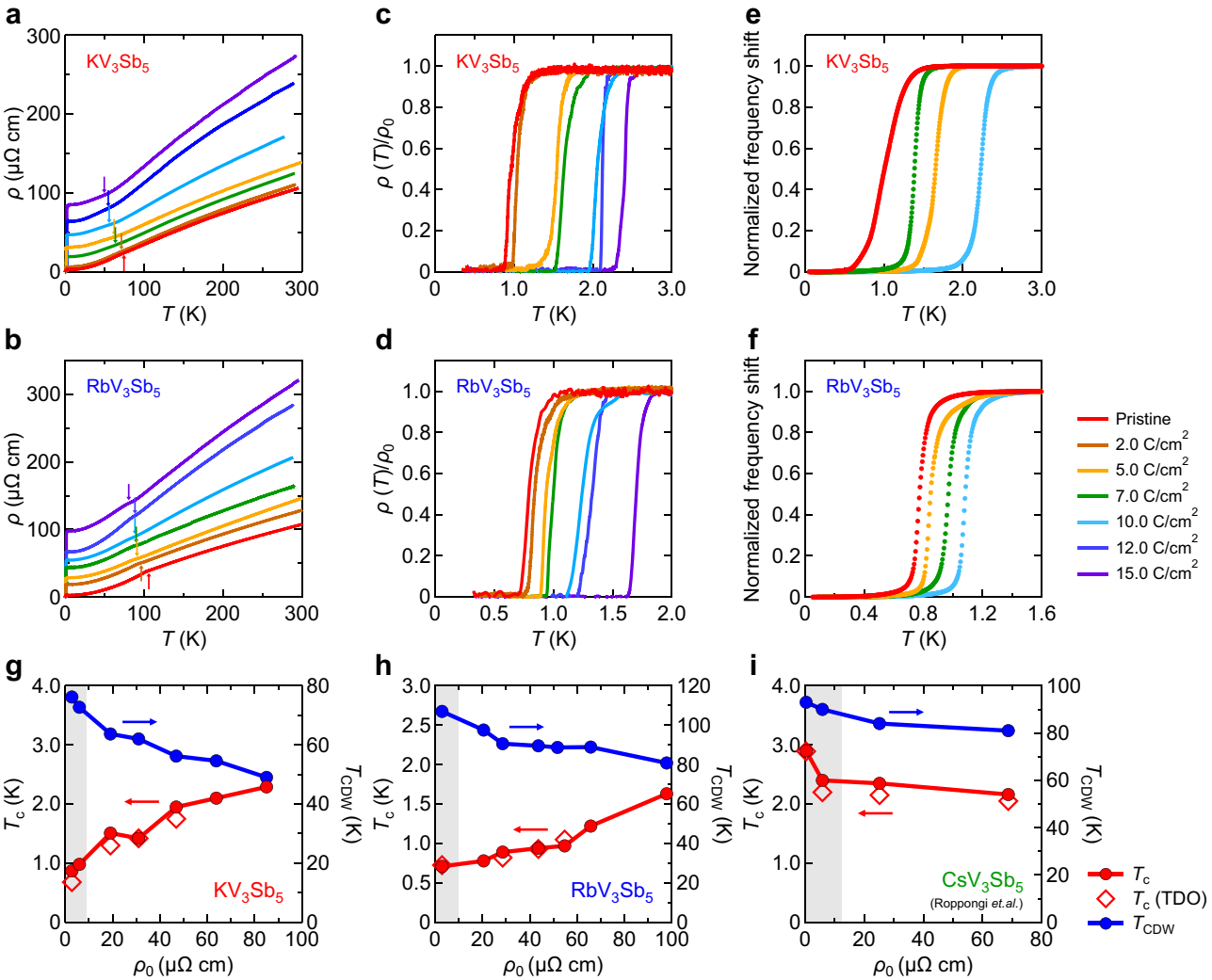

Fig. 2 | Impurity effects on the transition temperatures in AV_3Sb_5 (A = K, Rb, Cs). Temperature dependence of the electrical resistivity $\rho(T)$ for various electron irradiation doses in KV_3Sb_5 (**a**) and RbV_3Sb_5 (**b**). Arrows indicate the charge-density-wave (CDW) transition temperatures T_{CDW}. $\rho(T)$ normalized by the residual resistivity ρ_0 around the superconducting transition in pristine and irradiated KV_3Sb_5 (**c**) and RbV_3Sb_5 (**d**). Temperature dependence of the normalized frequency shift in the tunnel diode oscillator(TDO) measurements for various irradiation doses in KV_3Sb_5 (**e**) and RbV_3Sb_5 (**f**). Changes in superconducting (SC) transition temperature T_c and T_{CDW} as a function of ρ_0 in KV_3Sb_5 (**g**), RbV_3Sb_5 (**h**), and CsV_3Sb_5 (**i**). T_c is obtained from the resistivity (filled red circles) and TDO measurements (open red diamonds). T_{CDW} (filled brue circles) is determined from the resistivity measurements as a temperature at which $d\rho/dT$ exhibits dip (see Supplementary Note 4). The gray region represents the parameter space where SC with sign-changing order parameters is expected to survive based on the Abrikosov-Gor'kov (AG) therory. This region is determined using the pair-breaking parameter $g = \hbar/\tau_{imp}k_BT_{c0}$, where $\hbar$ is the reduced planck constant, $\tau_{imp} = \mu_0\lambda^2(0)/\rho_0$, μ_0 is the permeability of vacuum, $\lambda(0)$ is the penetration depth at zero temperature, k_B is the Boltzmann constant, and T_{c0} is the SC transition temperature of the pristine sample. We estimate $\lambda(0)$ from the μSR measurements[39,44].

represents the temperature dependence of the normalized frequency shift in the TDO for all alkali compounds. We note that the data of CsV_3Sb_5 are taken from the previous study[37]. A slightly broad SC transition in Fig. 1d may be related to the SC phase fluctuations or a short skin depth. Figure 1g summarizes T_c in AV_3Sb_5, determined from the temperature dependence of the normalized superfluid density $\rho_s(T)$, which is derived from the change in the penetration depth $\Delta\lambda(T)$, as in the case of CsV_3Sb_5[37]. Figure 1e shows $\Delta\lambda(T)$ normalized by the $0.5T_c$ value in the pristine AV_3Sb_5 samples. As clearly seen, CsV_3Sb_5 shows larger excitations at low temperatures compared to K/RbV_3Sb_5. To evaluate the temperature dependence of these results more quantitatively, we fitted the data below $T/T_c < 0.3$ with a power-law function, $\Delta\lambda(T) \propto T^n$, where $n \leq 2$ ($n > 2$) implies a nodal (fully gapped) gap structure. The dashed lines in Fig. 1e represent the fitting curves, and the obtained exponent n values are summarized in Fig. 1f. The result of $n > 2$ for all AV_3Sb_5 compounds suggests that the fully-gapped SC is universally realized in the AV_3Sb_5 family. It is worth noting that this result contradicts the μSR study suggesting a nodal gap structure in K/RbV_3Sb_5[44]. The discrepancy between our results and the previous report is discussed in Supplementary Note 1. More importantly, although all alkali compounds exhibit fully gapped behaviors, $\Delta\lambda(T)$ substantially differs between K/RbV_3Sb_5 and CsV_3Sb_5. To clarify the differences, we fitted $\Delta\lambda(T)$ below $0.3T_c$ with a fully gapped model, $\Delta\lambda(T) \propto T^{-1/2}\exp(-\Delta_0/k_BT)$, where Δ_0 is the gap minima in the momentum space and k_B is the Boltzmann constant. The obtained Δ_0/k_BT_c values are also depicted in Fig. 1f, signifying that Δ_0/k_BT_c in K/RbV_3Sb_5 is clearly larger than that in CsV_3Sb_5. Considering that an anisotropic gap structure makes the Δ_0 value smaller, our results of the pristine AV_3Sb_5 samples indicate that the gap structure in K/RbV_3Sb_5 is more isotropic than in CsV_3Sb_5.

Impurity effects

Next, we focus on the impurity effects on T_c and T_{CDW}. Figure 2a, b shows the temperature dependence of electrical resistivity $\rho(T)$ in pristine and

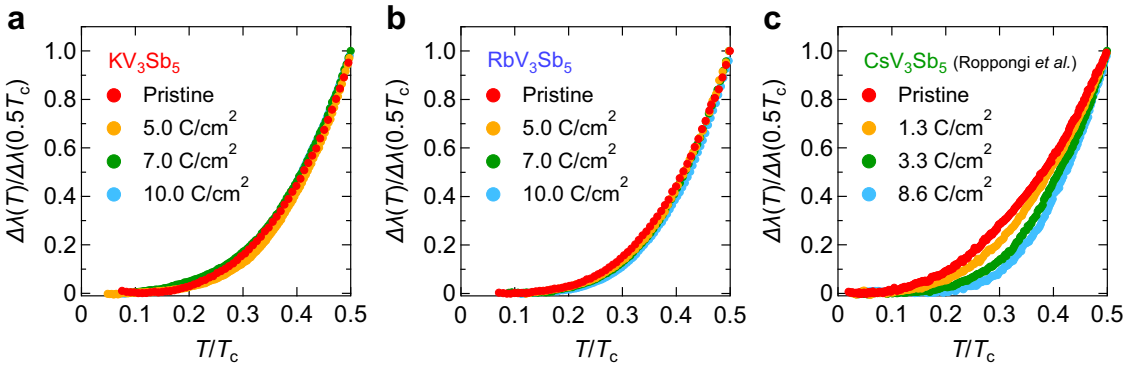

Fig. 3 | Impurity effects on the temperature dependence of the penetration depth. Temperature dependence of the penetration depth below $0.5T_c$ normalized by the value at $0.5T_c$ for various irradiation doses in KV_3Sb_5 (**a**), RbV_3Sb_5 (**b**), and CsV_3Sb_5 (**c**), where T_c is the superconducting transition temperature.

electron-irradiated samples of KV_3Sb_5 and RbV_3Sb_5, respectively. The resistivity progressively increases with irradiation, suggesting the successive introduction of homogeneous impurities by electron irradiation. Defining T_{CDW} from an anomaly in $d\rho(T)/dT$ as depicted by arrows in Supplementary Fig. S4a, b, a clear decrease in T_{CDW} with increasing impurity scattering can be observed in both the K and Rb cases, reminiscent of the case in CsV_3Sb_5. Focusing on the low-T behavior of $\rho(T)$ in Fig. 2c, d, on the other hand, T_c shows a clear increase with irradiation in contrast to T_{CDW}, which is a completely opposite behavior to the CsV_3Sb_5 case where T_c is suppressed by irradiation. The increase in T_c with disorder is also confirmed by the TDO measurements, as shown in Fig. 2e, f. Figure 2g–i summarizes T_c and T_{CDW} as a function of residual resistivity ρ_0 for A = K, Rb, and Cs, respectively. For all compounds, SC survives beyond the ρ_0 range where the SC with sign changing in gap functions can survive by the Abrikosov-Gor'kov theory (gray regions in Fig. 2g–i). This result rules out the SC states with symmetry-protected sign changing gap, such as chiral d-wave, p-wave, and f-wave pairing states. From the perspective of the relationship between SC and CDW orders, the opposite trend with decreasing T_{CDW} and increasing T_c indicates strong competition between SC and CDW states. A similar competition has been reported in some cuprates and TMDs[45,46]. However, the origin of the opposite behavior between K/RbV_3Sb_5 and CsV_3Sb_5 even with the similar electronic structure is nontrivial, which will be discussed later.

The impurity effects on the gap structure can be discussed from the evolution in the low-T behavior of $\Delta\lambda(T)$ against electron irradiation, as shown in Fig. 3. As reported in ref. 37, the gap structure in CsV_3Sb_5 significantly changes with irradiation, indicating that the anisotropic gap structure in the pristine sample becomes more isotropic by impurity scattering via the gap averaging effect in the momentum space. This can be seen in $\Delta\lambda(T)$ shown in Fig. 3c, where flattening behaviors are observed at low temperatures in irradiated samples. In K/RbV_3Sb_5, on the other hand, $\Delta\lambda(T)$ remains intact against impurity scattering (Fig. 3a, b), which is consistent with the more isotropic gap structure. This is because when the gap structure of the pristine sample is isotropic, the gap averaging effect can no longer play a role. Furthermore, since $\Delta\lambda(T) \propto T^2$ is expected to be caused by the impurity-induced low-energy Andreev bound states in the dirty SC state with sign-changing gap function, the observed robust behavior of $\Delta\lambda(T)$ with exponential T dependence against impurities provides strong evidence for an isotropic sign-preserving SC gap structure in both KV_3Sb_5 and RbV_3Sb_5.

Discussion

The opposite trend of T_c against irradiation between K/RbV_3Sb_5 and CsV_3Sb_5 can be explained as follows based on the observed SC gap structure. Whether T_c increases or decreases with impurities is determined by the balance of two contributions; one is the relationship between SC and coexisting electronic orders, and the other is the gap-averaging effect in the momentum space. Here, the former increases T_c when the order competing with SC is suppressed, and the latter decreases T_c. From $\Delta\lambda(T)$ shown in Fig. 3, the gap-averaging effect is substantial in CsV_3Sb_5, while that in K/RbV_3Sb_5 is relatively weak. Therefore, although the latter contribution, which reduces T_c, plays a significant role in CsV_3Sb_5, we can purely detect the former contribution originating from the intense competition between SC and CDW orders in K/RbV_3Sb_5. Here it should be noted that we do not consider an impurity-induced change of the CDW pattern in CsV_3Sb_5 because the amount of impurity introduced by irradiation is low enough to maintain the double-peak structure of the SC phase in the P-T phase diagram[37].

Having established the isotropic s-wave SC without sign reversal in the gap function in K/RbV_3Sb_5, we now discuss ingredients inducing the difference in gap anisotropy between K/RbV_3Sb_5 and CsV_3Sb_5. One possibility is the sample quality of the pristine samples since ρ_0 is lowest in CsV_3Sb_5. Indeed, while ρ_0 of CsV_3Sb_5 in ref. 37 is as small as 0.4 μΩcm, ρ_0 of KV_3Sb_5 and RbV_3Sb_5 in this study is 2.8 and 2.9 μΩcm. However, although the 1.3 C/cm^2 electron-irradiated CsV_3Sb_5 shows ρ_0 = 5.9 μΩcm[37], which is higher than the values in the pristine K/RbV_3Sb_5 samples, this sample still exhibits a much smaller value $\Delta_0/k_BT_c \approx 0.65$ showing stronger anisotropy than in the pristine K/RbV_3Sb_5 samples. Therefore, the impurity effects cannot wholly explain the isotropic gap structure in K/RbV_3Sb_5.

Alternatively, we focus on the reconstructions of the band structures in AV_3Sb_5 induced by the distinct $2 \times 2 \times 2$ BO states. We consider the p-type conduction band composed of the d_{xz}-orbitals. In the original kagome lattice model in the absence of the BO, the p-type band possesses three vHS points at M-points of the original Brillouin zone (BZ). The energy of the vHS points is slightly below the Fermi level; $E_{vHS} \approx -0.06$ eV for KV_3Sb_5, $E_{vHS} \approx -0.08$ eV for RbV_3Sb_5, and $E_{vHS} \approx -0.1$ eV for CsV_3Sb_5. The p-type band near the vHS points with large d_{xz}-orbital DOS plays an essential role in the emergence of CDW orders (such as the BO and the loop-current order) as well as the SC[4,5].

Figure 4a shows the 2×2 BO in the d_{xz}-orbital kagome lattice model with hopping modulations $\delta t \neq 0$: the TrH ($\delta t > 0$) and the SoD ($\delta t < 0$) BO states. In these BO states, three vHS points are moved to the same Γ-point in the folded BZ, forming a newly reconstructed band structure made of d_{xz}-orbitals. Below, we analyze a three-dimensional d_{xz}-orbital model with the kagome lattice given in Fig. 4a for simplicity. The in-plane nearest-neighbor hopping integral is $t = -0.5$ eV, and the inter-layer hopping integral $t^\perp$ is much smaller than $0.01|t|$ in magnitude. Hereafter, we set $t^\perp \to 0$ to simplify the discussion. Figure 4b shows the band structure at the $k_z = 0$ plane without the BO, while Fig. 4c–e shows the band structure at the $k_z = 0$ in the π-shifted TrH-TrH, π-shifted SoD-SoD, and vertically stacked TrH-SoD BO states, respectively. (Here, we set the BO parameter $|\delta t| = 0.015$ eV for each layer.) The corresponding Fermi surfaces are shown in Fig. 4f–i, respectively. In the absence of the BO, six vHS energy levels are almost degenerated ($E_{vHS} \approx -0.05$ eV), composing two small d_{xz}-orbital Fermi pockets with large DOS, as shown in Fig. 4f. In the TrH-TrH ($\delta t > 0$) and the SoD-SoD ($\delta t < 0$) BO states, nearly sixfold degenerated vHS energy levels split into fourfold states at $E_{vHS} - 2\delta t$ and twofold states at $E_{vHS} + 4\delta t$. In the TrH-TrH BO state, the hybridization gap appears around Γ point for

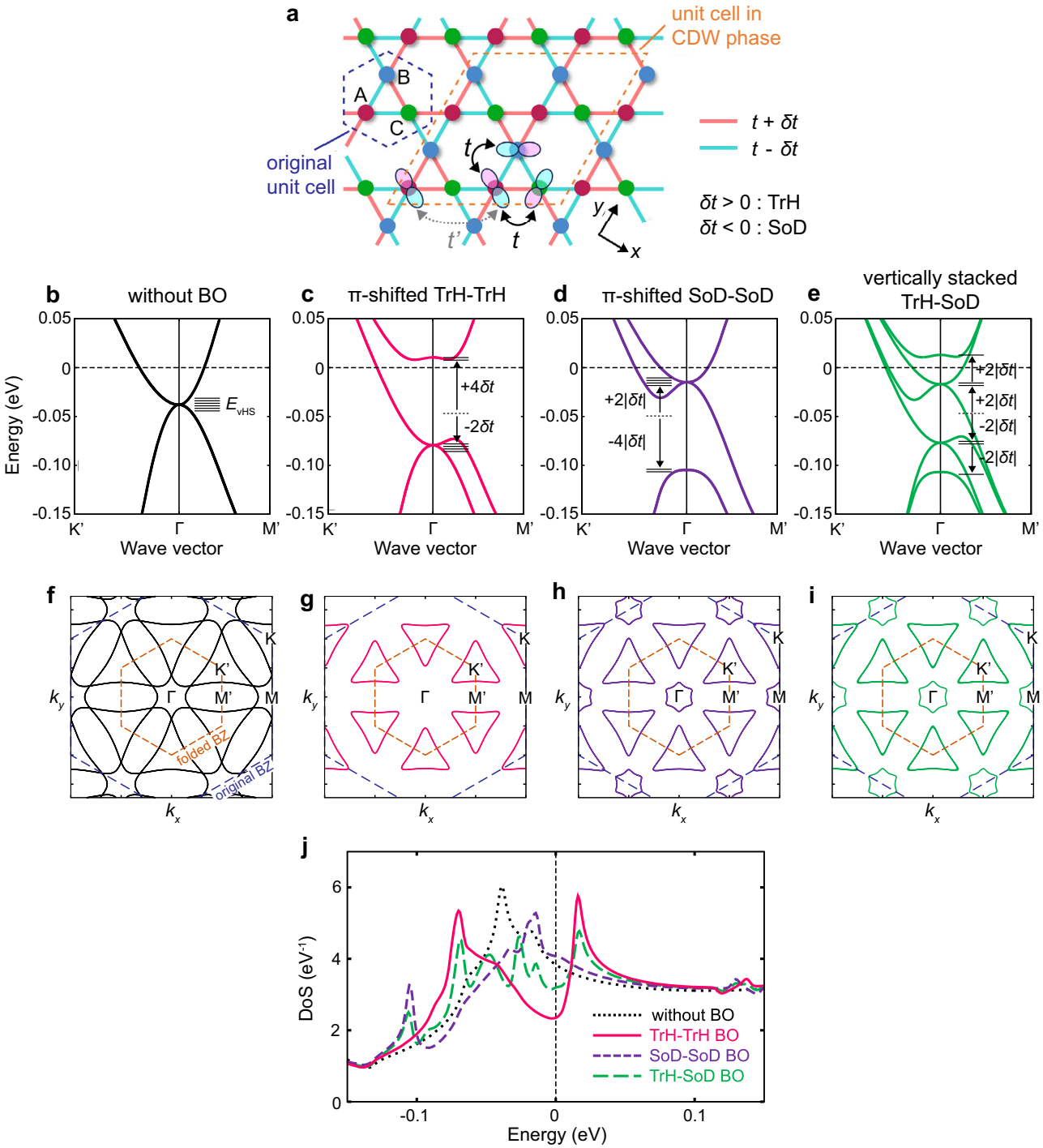

Fig. 4 | Band structures in the bond-order (BO) states calculated by d_{xz}-orbital kagome lattice model. a Tri-hexagonal (TrH) BO ($\delta t > 0$) and Star of David (SoD) BO ($\delta t < 0$) in the two-dimensional d_{xz}-orbital kagome lattice model. Hopping integrals are shown. Band structure at the $k_z = 0$ plane without BO (**b**), and with TrH-TrH BO (**c**), SoD-SoD BO (**d**), and TrH-SoD BO (**e**). Here, we put the inter-layer hopping integral $t^{\perp} \to 0$ to simplify the discussion. We set BO parameter $|\delta t| = 0.015$ eV in (**c**–**e**). Fermi surfaces without BO (**f**), and with π-shifted TrH-TrH BO (**g**), π-shifted SoD-SoD BO (**h**), and vertically stacked TrH-SoD BO (**i**). **j** d_{xz}-orbital density of states (DoS) in the TrH-TrH BO, SoD-SoD BO, TrH-SoD BO states for $|\delta t| = 0.015$ eV.

$4|\delta t| \gtrsim |E_{\mathrm{vHS}}|$, so the two small Fermi pockets disappear, as shown in Fig. 4g. In the TrH-SoD BO state shown in Fig. 4e, six vHS energy levels splits into two single states at $E_{\mathrm{vHS}} \pm 4\delta t$ and two twofold states at $E_{\mathrm{vHS}} \pm 2\delta t$. In this case, single small Fermi pocket survives even for $4|\delta t| \gtrsim |E_{\mathrm{vHS}}|$, as shown in Fig. 4i. We note that this characteristic split of vHSs is also observed in the first-principles calculations shown in Supplementary Note 5. However, it should be noted that folded Fermi pockets are generally difficult to observe in the photoemission spectroscopy due to their intrinsically weak intensity.

Figure 4j compares the d_{xz}-orbital DOS in the three (TrH-TrH, SoD-SoD, TrH-SoD) $2 \times 2 \times 2$ BO states. Here, we analyze the three-dimensional (d_{xz}, d_{yz})-orbital kagome lattice model introduced in ref. 49 to obtain realistic DOS. In the TrH-TrH BO state, the DOS at the Fermi level is reduced by forming the hybridization gap around Γ-point, while the DOS is essentially unchanged in the SoD-SoD phase. In the TrH-SoD BO state, the DOS at the Fermi level is also reduced by disappearing one of two Fermi pockets around Γ-point. Therefore, we theoretically revealed that the emergent d_{xz}-orbital

band structure strongly depends on the three-dimensional BO structure. Note that the d_{xz}-orbital DOS at the Fermi level is about 25% of the total $d+p$-orbital DOS according to the first-principles study for AV_3Sb_5.

Considering the reported differences in the CDW patterns (the TrH-TrH state in K/RbV$_3$Sb$_5$ and the TrH-SoD state in CsV$_3$Sb$_5$)[27–33], the small Fermi pockets around the folded Γ-point composed of the three vHS states survive only in CsV$_3$Sb$_5$ at low temperatures. Note that the above arguments are still valid even if a $2 \times 2 \times 4$ BO state is realized in CsV$_3$Sb$_5$ because the presence of the SoD layer is critical to maintain the vHS states around the folded Γ-point. Theoretically, the d_{xz}-orbital vHS states play an essential role in the quantum fluctuations and SC[4,5]. Therefore, although the stacking pattern of BO in our samples is not experimentally confirmed, we expect substantial BO fluctuations derived by the d_{xz}-orbital vHSs and associated electron correlations only in CsV$_3$Sb$_5$, which induce an anisotropic gap structure in CsV$_3$Sb$_5$ in contrast to an isotropic gap in K/RbV$_3$Sb$_5$. Furthermore, T_c of CsV$_3$Sb$_5$ is more than two times higher than that of K/RbV$_3$Sb$_5$ (Fig. 1g) even though the values of Sommerfeld coefficient γ indicate comparable DOS among AV_3Sb_5, as depicted in Fig. 1h, evidencing the critical role of the BO fluctuations to enhance T_c in kagome superconductors. Our conclusion implies that the double-peak structure of T_c in the P-T and hole-doped phase diagrams of CsV$_3$Sb$_5$ may be related to a change in the CDW patterns and associated BO fluctuations across the peak within the BO phase.

Here, we should mention a theoretical study of impurity effects on kagome materials suggesting that sign-changing gap symmetries, including d-wave, and chiral d-wave states are robust against nonmagnetic disorder because of the sublattice polarization of Fermi surfaces[50]. However, this argument is valid when defects on only the V sites are taken into account, and, in other words, defects in the alkali and Sb sites may destroy the sign-changing SC state. Indeed, we can expect a large number of defects on the alkali and Sb sites induced by electron irradiation (see Supplementary Note 3), and the observed T_c reduction in CsV$_3$Sb$_5$[37] evidences a finite pair-breaking effect of the nonmagnetic impurities. Moreover, the gap averaging effect of the impurity scatterings observed in CsV$_3$Sb$_5$ cannot be explained by the symmetry-protected gap structures. Therefore, our discussion about the gap symmetry in AV_3Sb_5 is still valid even with the orbital-polarized Fermi surfaces.

It has also been proposed that the vHS derived from the d_{xy} orbital may contribute to CDW formation[51,52]. While the strong electron correlation of the d_{xz} orbital, which gives the largest DOS near the Fermi level, plays the dominant role, the d_{xy} orbital may also assist the CDW cooperatively via intersite Coulomb or electron-phonon interactions.

Conclusions

In conclusion, we have studied the impurity effects on the SC gap structure and transition temperature in K/RbV$_3$Sb$_5$ from the penetration depth measurements and electron irradiation. By combining our results and the previous report on CsV$_3$Sb$_5$, we provide a comprehensive understanding of the SC gap structure in AV_3Sb_5 (A = K, Rb, Cs): quite anisotropic gap in CsV$_3$Sb$_5$ and isotropic gap in K/RbV$_3$Sb$_5$. Taking into account the differences in the band structures, it turns out that the vHSs essential for BO fluctuations depend sensitively on the patterns of CDW. Significantly developed BO fluctuations in CsV$_3$Sb$_5$ with the SoD pattern play a crucial role in inducing the strong SC gap anisotropy and the relatively high T_c. Furthermore, T_c and T_{CDW} clearly show opposite trends against disorder, suggesting intense competition between SC and CDW phases. Our systematic studies on AV_3Sb_5 shed new light on the interplay between unconventional s-wave SC and CDW orders in kagome materials and hopefully promote further exploration of novel physics originating from an interplay of exotic orders in kagome systems.

Methods

Single crystal growth

High-quality single crystals of K/RbV$_3$Sb$_5$ were grown by a modified self flux method using K ingot (Alfa, 99.95%), V powder (Sigma, 99.9%), and Sb shot (Alfa, 99.999%) for KV$_3$Sb$_5$ and Rb ingot (Alfa, 99.75%), V powder (Sigma, 99.9%,) and As shot (Alfa, 99.999%) for RbV$_3$Sb$_5$, respectively. The mixture was placed in an alumina crucible, which was then sealed in a quartz ampoule under high vacuum. The sealed ampoule was heated to 1000 °C, soaked at this temperature for 24 hours, and subsequently cooled down. Single crystals were then mechanically extracted from the flux. All preparation steps, except for the sealing and heating processes, were carried out in an argon glovebox.

Magnetic penetration depth measurement

The temperature dependence of the penetration depth was measured by the tunnel diode oscillator (TDO) technique at 13.8 MHz in a dilution refrigerator. The sample was put at the center of a coil forming the TDO circuit, and the relative change of the penetration depth $\Delta\lambda(T) = \lambda(T) - \lambda(0)$ is directly obtained from the shift of the resonant frequency of the TDO circuit $\Delta f(T)$ with the relation $\Delta\lambda(T) = G\Delta f(T) = G\{f(T) - f(0)\}$, where the geometrical constant G is determined by the shape of the sample. Here, the magnetic field induced by the coil is perpendicular to the kagome planes with a magnitude of the order of μT, which is much lower than the lower critical filed of the order of mT, confirming the Meissner state of our samples.

Electrical resistivity measurement

The electrical resistivity was measured by the four-terminal method with dc current applied within the ab plane in a ^{3}He refrigerator for $T < 5$ K and in a home-made probe for $T > 4.2$ K. The delta-mode of Keithley model 6221 and 2182A was used to eliminate the offset of dc resistivity. We confirmed that the applied current was low enough that the Joule heating can be ignored.

Electron irradiation

Electron irradiation with the incident energy of 2.5 MeV was performed on the SIRIUS Pelletron accelerator in Laboratoire des Solides Irradies (LSI) at Ecole Polytechnique. Here, energy transfer from the irradiated electrons to the lattice exceeds threshold energy for the formation of vacancy-interstitial Frenkel pairs, which act as point defects. We performed irradiation around 20 K to prevent the defect migration and agglomeration. Although partial annealing of the introduced defects occurs on warming to the room temperature, uniform point defects are kept due to the lower migration energy. Electron irradiation has no pressure or doping effect since it does not change the lattice constants and carrier density.

Theoretical calculations

In this study, we analyze an effective Hamiltonian model based on an extended unit cell with 24 sites[49]. Each unit cell consists of two layers, with 12 V sites per layer. The Hamiltonian is given by:

$$H = \sum_{i,j,l,m,\sigma} t_{i,j}^{l,m} c_{i,l,\sigma}^{\dagger} c_{j,m,\sigma} + \sum_{<i,j>,l,m,\sigma} \delta t_{i,j} c_{i,xz,\sigma}^{\dagger} c_{j,xz,\sigma}.$$

Here, $c_{i,l,\sigma}^{\dagger}$ is the creation operator for a spin-σ electron in orbital l (either d_{xz} or d_{yz}) on the i-th site (i = 1–24). The hopping parameters $t_{i,j}^{l,m}$ are chosen to approximately reproduce the three-dimensional Fermi surface obtained from first-principles calculations. Specifically, the onsite energy of the d_{yz} orbital is set to 2.3. The nearest-neighbor hoppings are set as follows: $t = -0.5$ for intra-orbital d_{xz} hopping, $t_{yz} = -1$ for d_{yz}, and $t_{xz\text{-}yz} = \pm 0.05$ for inter-orbital d_{xz}-d_{yz} hopping. The hopping across two sites within the d_{xz} orbital is set to $t\prime = -0.08$ (see Fig. 4a). We set interlayer hopping of the intra-d_{yz} orbital $t_{yz,yz}^{\perp} = 0.02$ for the site directly above and those belonging to the same triangle. The interlayer hopping for the d_{xz} orbital is neglected due to its small magnitude. The unit for all hopping parameters is eV.

The bond order is introduced as a modulation of the nearest-neighbor hopping in the d_{xz} orbital, $\delta t_{i,j}^{b} = \pm \delta t$, with the modulation pattern shown in Fig. 4a.

For Fig. 4, we used a $240 \times 240 \times 120$ k-mesh. The electron number was set to $N = 17.8$. For Fig. 4b–i, in order to clarify the changes in the band structure and Fermi surface, we used a single-orbital model with only the d_{xz} orbital and set $N = 11.6$.

Data availability

The data that support the findings of this study are available within the paper and its Supplementary Information. Source data are provided with this paper as Supplementary Data 1.

Code availability

The codes used for the numerical calculations are available from the corresponding authors upon reasonable request. The commercially available WIEN2k software was also used for the first principles calculations presented in the Supplementary Information.

Received: 12 February 2025; Accepted: 8 July 2025;
Published online: 18 July 2025

References

1. Wang, W.-S., Li, Z.-Z., Xiang, Y.-Y. & Wang, Q.-H. Competing electronic orders on kagome lattices at van Hove filling. *Phys. Rev. B* **87**, 115135 (2013).
2. Kiesel, M. L., Platt, C. & Thomale, R. Unconventional Fermi surface instabilities in the kagome hubbard model. *Phys. Rev. Lett.* **110**, 126405 (2013).
3. Wu, X. et al. Nature of unconventional pairing in the kagome superconductors AV_3Sb_5 (A = K, Rb, Cs). *Phys. Rev. Lett.* **127**, 177001 (2021).
4. Tazai, R., Yamakawa, Y., Onari, S. & Kontani, H. Mechanism of exotic density-wave and beyond-Migdal unconventional superconductivity in kagome metal AV_3Sb_5 (A = K, Rb, Cs). *Sci. Adv.* **8**, eabl4108 (2022).
5. Tazai, R., Yamakawa, Y. & Kontani, H. Charge-loop current order and Z_3 nematicity mediated by bond order fluctuations in kagome metals. *Nat. Commun.* **14**, 7845 (2023).
6. Wilson, S. D. & Ortiz, B. R. AV_3Sb_5 kagome superconductors. *Nat. Rev. Mater.* **9**, 420–432 (2024).
7. Ortiz, B. R. et al. CsV_3Sb_5: a $\mathbb{Z}_2$ topological kagome metal with a superconducting ground state. *Phys. Rev. Lett.* **125**, 247002 (2020).
8. Ortiz, B. R. et al. Superconductivity in the $\mathbb{Z}_2$ kagome metal KV_3Sb_5. *Phys. Rev. Mater.* **5**, 034801 (2021).
9. Yin, Q. et al. Superconductivity and normal-state properties of kagome metal RbV_3Sb_5 single crystals. *Chin. Phys. Lett.* **38**, 037403 (2021).
10. Du, F. et al. Pressure-induced double superconducting domes and charge instability in the kagome metal KV_3Sb_5. *Phys. Rev. B* **103**, L220504 (2021).
11. Wang, N. N. et al. Competition between charge-density-wave and superconductivity in the kagome metal RbV_3Sb_5. *Phys. Rev. Res.* **3**, 043018 (2021).
12. Chen, K. Y. et al. Double superconducting dome and triple enhancement of T_c in the kagome superconductor CsV_3Sb_5 under high pressure. *Phys. Rev. Lett.* **126**, 247001 (2021).
13. Yu, F. H. et al. Unusual competition of superconductivity and charge-density-wave state in a compressed topological kagome metal. *Nat. Commun.* **12**, 3645 (2021).
14. Yang, S.-Y. et al. Giant, unconventional anomalous Hall effect in the metallic frustrated magnet candidate, KV_3Sb_5. *Sci. Adv.* **6**, eabb6003 (2020).
15. Jiang, Y.-X. et al. Unconventional chiral charge order in kagome superconductor KV_3Sb_5. *Nat. Mater.* **20**, 1353–1357 (2021).
16. Guo, C. et al. Switchable chiral transport in charge-ordered kagome metal CsV_3Sb_5. *Nature* **611**, 461–466 (2022).
17. Mielke, C. et al. Time-reversal symmetry-breaking charge order in a kagome superconductor. *Nature* **602**, 245–250 (2022).
18. Xu, Y. et al. Three-state nematicity and magneto-optical Kerr effect in the charge density waves in kagome superconductors. *Nat. Phys.* **18**, 1470–1475 (2022).
19. Asaba, T. et al. Evidence for an odd-parity nematic phase above the charge-density-wave transition in a kagome metal. *Nat. Phys.* **20**, 40–46 (2024).
20. Zhao, H. et al. Cascade of correlated electron states in the kagome superconductor CsV_3Sb_5. *Nature* **599**, 216–221 (2021).
21. Xiang, Y. et al. Twofold symmetry of c-axis resistivity in topological kagome superconductor CsV_3Sb_5 with in-plane rotating magnetic field. *Nat. Commun.* **12**, 6727 (2021).
22. Li, H. et al. Rotation symmetry breaking in the normal state of a kagome superconductor KV_3Sb_5. *Nat. Phys.* **18**, 265–270 (2022).
23. Nie, L. et al. Charge-density-wave-driven electronic nematicity in a kagome superconductor. *Nature* **604**, 59–64 (2022).
24. Li, H. et al. Unidirectional coherent quasiparticles in the high-temperature rotational symmetry broken phase of AV_3Sb_5 kagome superconductors. *Nat. Phys.* **19**, 637–643 (2023).
25. Tazai, R., Yamakawa, Y. & Kontani, H. Drastic magnetic-field-induced chiral current order and emergent current-bond-field interplay in kagome metals. *Proc. Natl Acad. Sci.* **121**, e2303476121 (2024).
26. Shumiya, N. et al. Intrinsic nature of chiral charge order in the kagome superconductor RbV_3Sb_5. *Phys. Rev. B* **104**, 035131 (2021).
27. Kang, M. et al. Charge order landscape and competition with superconductivity in kagome metals. *Nat. Mater.* **22**, 186–193 (2023).
28. Kautzsch, L. et al. Structural evolution of the kagome superconductors AV_3Sb_5 (A = K, Rb, Cs) through charge density wave order. *Phys. Rev. Mater.* **7**, 024806 (2023).
29. Kato, T. et al. Three-dimensional energy gap and origin of charge-density wave in kagome superconductor KV_3Sb_5. *Commun. Mater.* **3**, 30 (2022).
30. Frassineti, J. et al. Microscopic nature of the charge-density wave in the kagome superconductor RbV_3Sb_5. *Phys. Rev. Res.* **5**, L012017 (2023).
31. Ortiz, B. R. et al. Fermi surface mapping and the nature of charge-density-wave order in the kagome superconductor CsV_3Sb_5. *Phys. Rev. X* **11**, 041030 (2021).
32. Li, C. et al. Coexistence of two intertwined charge density waves in a kagome system. *Phys. Rev. Res.* **4**, 033072 (2022).
33. Hu, Y. et al. Coexistence of trihexagonal and star-of-david pattern in the charge density wave of the kagome superconductor AV_3Sb_5. *Phys. Rev. B* **106**, L241106 (2022).
34. Oey, Y. M., Kaboudvand, F., Ortiz, B. R., Seshadri, R. & Wilson, S. D. Tuning charge density wave order and superconductivity in the kagome metals $KV_3Sb_{5-x}Sn_x$ and $KV_3Sb_{5-x}Sn_x$. *Phys. Rev. Mater.* **6**, 074802 (2022).
35. Oey, Y. M. et al. Fermi level tuning and double-dome superconductivity in the kagome metal $CsV_3Sb_{5-x}Sn_x$. *Phys. Rev. Mater.* **6**, L041801 (2022).
36. Zheng, L. et al. Emergent charge order in pressurized kagome superconductor CsV_3Sb_5. *Nature* **611**, 682–687 (2022).
37. Roppongi, M. et al. Bulk evidence of anisotropic s-wave pairing with no sign change in the kagome superconductor CsV_3Sb_5. *Nat. Commun.* **14**, 667 (2023).
38. Mu, C. et al. S-wave superconductivity in kagome metal CsV_3Sb_5 revealed by $^{121/123}$Sb NQR and ^{51}V NMR measurements. *Chin. Phys. Lett.* **38**, 077402 (2021).
39. Gupta, R. et al. Microscopic evidence for anisotropic multigap superconductivity in the CsV_3Sb_5 kagome superconductor. *npj Quantum Mater.* **7**, 49 (2022).
40. Xu, H.-S. et al. Multiband superconductivity with sign-preserving order parameter in kagome superconductor CsV_3Sb_5. *Phys. Rev. Lett.* **127**, 187004 (2021).

41. Duan, W. et al. Nodeless superconductivity in the kagome metal CsV_3Sb_5. *Sci. China Phys. Mech. Astron.* **64**, 107462 (2021).
42. Grant, M. J. et al. Superconducting energy gap structure of CsV_3Sb_5 from magnetic penetration depth measurements. *J. Phys. Condens. Matter* **37**, 065601 (2024).
43. Mine, A. et al. Direct observation of anisotropic Cooper pairing in kagome superconductor CsV_3Sb_5. Preprint at https://arxiv.org/abs/2404.18472 (2024).
44. Guguchia, Z. et al. Tunable unconventional kagome superconductivity in charge ordered RbV_3Sb_5 and KV_3Sb_5. *Nat. Commun.* **14**, 153 (2023).
45. Cho, K. et al. Using controlled disorder to probe the interplay between charge order and superconductivity in $NbSe_2$. *Nat. Commun.* **9**, 2796 (2018).
46. Leroux, M. et al. Disorder raises the critical temperature of a cuprate superconductor. *Proc. Natl Acad. Sci.* **116**, 10691–10697 (2019).
47. Mizukami, Y. et al. Disorder-induced topological change of the superconducting gap structure in iron pnictides. *Nat. Commun.* **5**, 5657 (2014).
48. Nagashima, T. et al. Lifting of gap nodes by disorder in tetragonal $FeSe_{1-x}S_x$ superconductors. *Phys. Rev. Lett.* **133**, 156506 (2024).
49. Tazai, R., Yamakawa, Y., Morimoto, T. & Kontani, H. Quantum-metric-induced giant and reversible nonreciprocal transport phenomena in chiral loop-current phases of kagome metals. Preprint at https://arxiv.org/abs/2408.04233 (2024).
50. Holbæk, S. C., Christensen, M. H., Kreisel, A. & Andersen, B. M. Unconventional superconductivity protected from disorder on the kagome lattice. *Phys. Rev. B* **108**, 144508 (2023).
51. Denner, M. M., Thomale, R. & Neupert, T. Analysis of charge order in the kagome metal AV_3Sb_5 (A = K, Rb, Cs). *Phys. Rev. Lett.* **127**, 217601 (2021).
52. Barman, C. K., Kim, S.-W. & Kim, Y. Stacking-dependent van Hove singularity shifts in three-dimensional charge density waves of kagome metals AV_3Sb_5 (A = K, Rb, Cs). *Curr. Appl. Phys.* **68**, 31–38 (2024).

Acknowledgements

This work was supported by Grants-in-Aid for Scientific Research (KAKENHI) (Nos. JP24K17007, JP24H01646, JP23H00089, JP22H00105), and Grant-in-Aid for Scientific Research for Transformative Research Areas (A) "Correlation Design Science" (No. JP25H01248) from Japan Society for the Promotion of Science (JSPS). Electron irradiation was conducted at the SIRIUS accelerator facility at École Polytechnique (Palaiseau, France) and was supported by EMIR&A French network (FR CNRS 3618) (proposal No. 22-8950). S.D.W. and A.C.S. gratefully acknowledge support via the UC Santa Barbara NSF Quantum Foundry funded via the Q-AMASE-i program under award DMR-1906325. Work by B. R. O. is supported by the U.S. Department of Energy, Office of Science, Basic Energy Sciences, Materials Sciences and Engineering Division.

Author contributions

K.H. and T.S. conceived the project. T.N., K.Ishihara, F.C., K.Imamura, M.R., K.H., and T.S. performed the magnetic penetration depth measurements and analyzed the results. R.G. and M.K. conducted electron irradiation experiments. B.R.O., A.C.S., and S.D.W. synthesized the single crystals. Y.Y., R.T., and H.K. performed the theoretical calculations. T.N., K.Ishihara, Y.Y., H.K., K.H., and T.S. prepared the manuscript. All authors discussed the experimental results.

Competing interests

The authors declare no competing interests.

Additional information

Supplementary information The online version contains supplementary material available at https://doi.org/10.1038/s42005-025-02225-8.

Correspondence and requests for materials should be addressed to Kota Ishihara or Takasada Shibauchi.

Peer review information *Communications Physics* thanks the anonymous reviewers for their contribution to the peer review of this work.